LBNL-55541

Materials Sciences Division, Lawrence Berkeley National Laboratory, and Department of Materials Science and Engineering, University of California at Berkeley

PROTECTIVE COATING ON STAINLESS STEEL INTERCONNECT FOR SOFCs: OXIDATION KINETICS AND ELECTRICAL PROPERTIES

[1]X. Chen, [1]P.Y. Hou, [1]C.P. Jacobson, [1]S.J. Visco, and L.C. De Jonghe[1,2]

[1]Materials Science Division, Lawrence Berkeley National Laboratory, and
Department of Materials Science and Engineering
University of California, Berkeley, CA 94720, USA

[1,2]Corresponding author:
Department of Materials Science and Engineering
324 Hearst Mining Building,
University of California, Berkeley, CA 94720-1760

Tel: (510) 486-6139; Fax: (510) 486-4881
E-mail address: LCDejonghe@lbl.gov (L.C. De Jonghe)

submitted May 2004

Solid State Ionics

Work supported by the Director, Office of Science, Office of Basic Energy Sciences, Division of Materials Sciences and Engineering of the U.S. Department of Energy under Contract No. DE-AC03-76SF00098.

PROTECTIVE COATING ON STAINLESS STEEL INTERCONNECT FOR SOFCs: OXIDATION KINETICS AND ELECTRICAL PROPERTIES

X. Chen, P.Y. Hou, C.P. Jacobson, S.J. Visco, and L.C. De Jonghe

Materials Sciences Division, Lawrence Berkeley National Laboratory, and
Department of Materials Science and Engineering, University of California, Berkeley, CA 94720

Abstract

An effective, dense and well adherent coating was produced on 430SS that has the result of significantly reducing the oxidation rate of this alloy at elevated temperatures. The coating is essentially a Mn-Co-O spinel, applied in powder form, and compacted to improve its green density. A simplified model is presented that allows an assessment of the effects of the contact and scale geometries. For 850^{o}C, an ASR can be predicted of approximately 0.5Ωcm^{2}, after 50,000hrs in air, taking into account a factor of 10 penalty for unfavorable contact geometries. The effect of the densified Mn-Co spinel coating is to reduce significantly Cr_2O_3 sub-scale formation, lower the thermal expansion mismatch, and increase the electronic conductivity of the scale.

The findings point to several potential remedies for achieving coatings on 430 SS that allow for metal interconnects with a service life of 50,000hrs or more. Considering contact geometries, such service life is unlikely to be possible above operating temperatures of about 700^{o}C, unless highly specialized alloys are used, with potential processing and cost penalties.

Keywords: Interconnect, Stainless steel, Cr_2O_3, SOFC, ASR

---

* Corresponding author. Tel: +1-510-486-6138; fax: +1-510-486-4881. *E-mail address:* lcdejonghe@lbl.gov (L.C. DeJonghe)
†Supported by the Director, Office of Science, Office of Basic Energy Sciences, Division of Materials Sciences and Engineering of the U.S. Department of Energy under Contract No. DE-AC03-76SF00098.

1. Introduction

Interconnects in solid oxide fuel cells (SOFCs) provide the electrical connection between the individual cells, as well as separate the anode form the cathode compartments. To properly function in SOFCs, the interconnect materials must possess a combination of physical and electrical properties:

1) High temperature oxidation resistance in both anode and cathode atmospheres

2) High electrical conductivity and negligible ionic conductivity

3) Thermal expansion compatibility with the other parts of the SOFC

4) Zero open porosity and sufficient mechanical strength

5) Chemical compatibility with the materials it contacts

6) Thermodynamic stability over the applied temperature range

Recently, significant progress has been made toward intermediate-temperature SOFCs (~800^{o}C), which can keep the cell power density and durability at the same level as those high temperature SOFCs. This progress is achieved by reducing the thickness of the conventional doped zirconia electrolytes [1-3] and/or by the development of new electrolytes with better oxide-ion conductivity than the traditional yttria stabilized zirconia (YSZ) [4-6]. At about 800^{o}C, high temperature oxidation-resistant ferritic steels are considered to be the most promising interconnect materials. Among these alloys, chromium based alloys [7-9] are mostly studied because they have a number of advantages: (1) The coefficient of thermal expansion, CTE, of ferritic Cr-based alloys is close to that of other cell components. For example, the CTEs of a LSM (lanthanum strontium manganate) and a 430 Fe-Cr alloy are 11-13x10^{-6} and 9-12x10^{-6} K^{-1}, respectively [10]. (2) Cr-based alloys, especially stainless steels such as the 430 or 446 ferritic alloys, are low cost and have excellent machinability. However, particularly in oxidizing

atmospheres, the formation of chromia scales leads to high contact resistances deleterious to the fuel cell performance. In addition, volatile Cr species can be released from the Cr_2O_3 scale, depending on the temperature and partial pressures of H_2O and O_2 [11]. The presence of the volatile chromium species, notably $CrO_2(OH)_2$, in the cathode of an SOFC is known to cause rapid cathode poisoning and performance degradation.[12] Improving the electrical properties of the oxide layer that forms on a metallic interconnect requires suppressing the formation of the resistive Cr_2O_3 phase, and promoting the formation of more conductive phases. Further, the transport of Cr to the gas-phase must be inhibited by a dense protective coating. The effectiveness of the coating must be maintained for very extended periods, e.g. 50,000hrs or more [13].

In the present work, a dense Mn-Co containing surface oxide coating is reported that was produced on a commercial 430 stainless steel, forming an electronically highly conductive, protective spinel, and involving solid-state reaction with Cr_2O_3 during oxidation of the steel. Solid-state reaction can be an economical process compared to plasma spraying or chemical vapor deposition. Previous studies by Huang *et al*. [14], indicated that the electronic conductivity of Cr_2O_3 can be improved by the incorporating and Co and Mn, as would result from the reaction with a Co-Mn oxide coating.

Quadakkers *et al.* [15] showed that a Mn-Cr-O spinel phase instead of Cr_2O_3 was formed as the contact layer between LSM cathode and the Cr-based alloy interconnect during oxidation due to solid-state and gas phase transport of chromium species. This transport led to the formation of a $CoCr_2O_4$ spinel when the coating was $LaCoO_3$, and to the formation of $MnCr_2O_4$ when the contacting material was LSM. The formation of this spinel near the interface with the Cr-based alloy can produce a local enrichment of La in the middle of the coating. As a result, La_2O_3 that is formed may hydrolyze in water containing atmospheres, leading to mechanical degradation of the coating. Early investigations by Wickham and Croft [15] and by Naka *et al.* [16] have shown that Mn-Co-O spinel has a high electronic conductivity, and could be a useful

electrode in a number of electrochemical devices. The high electronic conductivity follows when mixed valence ions are present on the same spinel sublattice, facilitating electron transport. Larring and Norby [17] reported that a Mn-Co-O spinel was able to reduce Cr interdiffusion significantly between a Plansee alloy and a contacting LSM/LSC (lanthanum strontium manganate/ lanthanum strontium cobaltate) mixed perovskite when it was introduced as an interlayer, also leading to an ASR (area specific resistance) of the metal/ceramic interface of only 0.024 ohmcm^2 after 10,000 hours at ~950^{0}C, in air. Badwal, *et al.* in a recent patent [18] reported oxide coatings containing at least one metal, M, selected from the transition series Mn, Fe, Co and Ni. An M-Cr spinel layer would develop between the metal substrate and the coating layer by the reaction of the oxide with the surface chromium oxide that forms on the alloy substrate.

The present work considers further the use of a Mn-Co-O spinel coating on a 430 stainless steel, forming a protective layer that slows the chromia scale formation significantly while maintaining a low interface resistance, and it examines its behavior under thermal cycling, and comments on the role of contact geometry. Possible mechanisms involved in the modifications to the oxidation kinetics are also discussed.

2. Experimental

2.1 Spinel coating powder preparation

$MnCr_2O_4$, $Mn_{1.5}Cr_{1.5}O_4$, $MnCrCoO_4$, and $MnCo_2O_4$ were prepared by a glycine nitrate combustion synthesis [19]. The molar ratio of glycine-to-metal ions was 2:1. After combustion, the spinel powder was calcined at 1100^{o}C in air, for 2 hours, to remove residual carbon. The powder was attritor-milled in isopropanol, for 1 hour, at 550 rpm. The various materials were compacted and sintered into pellets suitable for thermal expansion measurements by dilatometry and for electrical measurements.

2.2 Electrical properties determination

After drying, the attritor-milled spinel powders were compacted into pellets in a 2 cm diameter steel die, at about 70 MPa. The pellets were sintered at 1300^{o}C/4h in air, and their conductivities were determined every 50^{o}C by a four-probe method, similar to the one used by Huang *et al.* [14], but using gold rather than platinum paste. The results of the measurements, together with literature data on Cr_2O_3 conductivities [20], are shown in Fig. 1. The manganese cobalt spinel showed the highest electronic conductivity. Cr_2O_3 generally has a much lower electronic conductivity. Increasing the Cr contents of the spinel correlates with decreasing electronic conductivities for this spinel. This indicates that reaction of $MnCo_2O_4$ with Cr_2O_3 could be expected to lead to scales of improved conductivity. The $MnCo_2O_4$ spinel was therefore selected as the most promising coating material.

2.3 Coating method and oxidation heat treatments

A commercial ferritic 430 stainless steel (150μm thick) was selected for this study, because of its low cost, ready availability, and suitable chromium content. The composition, provided by the supplier, is shown in Table 1. The steel sheets were cut into 1cmx1cm square samples, and abraded on both sides with #1200 grit SiC sandpaper. A slurry was prepared by dispersing the attritor-milled spinel powders in IPA (isoproponal) together with 5wt% HPC (Hydroxypropyl cellulose). A strongly adherent coating could be produced by slurry-spraying the prepared steel surfaces, using an Iwata Eclipse HP-BCS spray gun. The as-deposited coatings were approximately 15-20 μm thick. To evaluate the effects of the green density of the coating, some coated samples were mechanically compressed to 70 MPa prior to heating.

Three types of samples were prepared,

Sample type A: Uncoated 430 stainless steel

Sample type B. 430 stainless steel coated with $MnCo_2O_4$

Sample type C: 430 stainless steel, coated with $MnCo_2O_4$ and mechanically compacted

The samples were heated first at 800^0C for an initial oxidation, for 60 hrs, in stagnant air. This treatment served to densify the sprayed-on coating, and to form an initial Cr_2O_3 scale. Following this initial oxidation, the samples were either held at 850^0C in air, or subjected to cyclic oxidation between room temperature and 850^0C with 30 min holds at temperature, to an additional cumulative exposure at 850^0C of 120 hrs. Heating and cooling rates were approximately 20^oC/min. Cyclic oxidation should be expected to lead to spalling and delamination of the scales if there are significant thermal expansion mismatches between the scale and the substrate alloy, particularly for thick coatings.

3. Results and discussions

3.1 Thermal expansion measurements.

The results of the differential thermal expansion measurements, with LSM as a reference, are listed in Table 2. The CTE of $MnCo_2O_4$ is nearly identical to that of LSM, while the incorporation of Co in $(Mn,Cr)_3O_4$ spinels significantly reduces the ΔCTE with LSM or 430 SS. A low ΔCTE is essential for forming scales that can adhere up to some large critical thickness.

3.2 Effects of coating compaction

Cross-sectional SEM (scanning electron microscope) images of Sample B and Sample C after the single initial oxidation in air at 800^0C, for 60 hrs, are compared in Fig. 2a and 2b. It is evident that the compaction of the as-deposited coating improved the density of the coating layer very significantly. Without this compaction, the as-deposited Mn-Co-O spray coating remains porous, providing poor protection. Therefore, the density of the deposited coating prior to firing

needs to be high, as may be achieved either by mechanical compaction or by alternative deposition processes such as electrophoresis. In this work, other coating application methods were not examined, and only mechanical compaction was pursued.

3.3. Oxidation Kinetics and cyclic oxidation

Samples of type A and C, after the initial oxidation, were suspended in a Cahn microbalance, in stagnant air, for 120 hrs, and weight gains were recorded over time after a constant temperature of 850^{o}C was reached. A second set of samples, after the initial oxidation at 800^{o}C, was subjected to cyclic oxidation between room temperature and 850^{o}C, with dwell times of approximately 30 min up to a cumulative exposure of 120hrs at 850^{o}C, and weight changes were recorded at room temperature every 2-5 cycles. Cooling/heating rates were approximately 20^{o}C/min. The oxidation results are shown in Fig. 3. Weight gain for the coated steel is reduced very significantly compared to the uncoated steel. Weight gain for the uncoated steel in cyclic oxidation was apparently low, but this was due to the extensive spalling of the oxide coating, and does not represent improved oxidation resistance. In contrast, the scale formed on the coated/compacted samples did not show any evidence of spalling, and remained fully adherent throughout the cyclic oxidation. The weight gain of the uncoated steel, sample type A, during the 850^{o}C oxidation, and of the coated/compacted samples (type C) during cyclic oxidation, could be fitted to a near parabolic relationship with time. This is expected when the oxide scale growth is controlled by diffusion of ions through a dense scale. A rate constant, k_g, given in Table 3, characterizing the rate of weight gain, $d\Delta W/dt$, as a result of oxidation can be defined by $(\Delta W)^2=k_g t$. The scale structure in the present case is complex and, as a result, a corresponding simple parabolic rate constant for the thickness increase can not be readily defined. For comparison of the different oxidation rates obtained by others, however, an effective parabolic rate constant, $k_{p\ eff}$, may be defined assuming that the weight gain is due entirely to the formation of a dense Cr_2O_3 layer, although part of this chromia scale will react with the coating.

With this assumption, and $k_{p,eff}$ in μm/√hour, $k_{p,eff}$ is defined by [14]:

$$k_{p\,eff} = 6.10^5\left(\frac{MW_{Cr_2O_3}}{(3/2)MW_{O_2}}.\frac{1}{\rho_{Cr_2O_3}}\right)\sqrt{k_g}.$$

where $MW_{Cr_2O_3}$ and MW_{O_3} are the molecular weights of chromia and oxygen, and $\rho_{Cr_2O_3}$ is the density of chromia (5.21g/cm^3), so that an approximate effective chromia scale thickness, $X_{Cr_2O_3}$ can be obtained from $X_{Cr_2O_3} = k_{p,eff}.\sqrt{t}$. These rate constants, Table 3, show that at 850^{o}C, the coated/compacted steel, sample type C, has a substantially reduced oxidation rate compared to the uncoated steel, sample type A. Extrapolation to a 50,000 hr exposure at 850^{o}C, with $k_{p\,eff}$= 4.4x10^{-2} μm/√hour would lead to an effective chromia scale thickness of about 10μm, compared to over 100μm for the unprotected steel (provided this scale would not spall off or be limited by Cr evaporation). The values of $k_{p\,eff}$ for the cyclic oxidation appear to be slightly higher because the heating and cooling periods are not accounted for. These results may be compared to the reduced oxidation rates reported by Zhu *et al.* [21] for a 444 stainless steel coated with a thin layer of $LaCrO_3$, involving r.f. sputtering and reaction or sol-gel coating, giving a k_g of about 5.8x10^{-14}g^{2}cm^{-4}s^{-1} or a $k_{p\,eff}$=8.7x10^{-2}μm/√hour at 800^{o}C, corresponding to a 50,000hr-800^{o}C projected effective chromia scale thickness of about 20μm. Huang *et al.* [14] reported that for an Ebrite alloy with an yttrium reactive element coating $k_{p\,eff}$ at 800^{o}C was 4x10^{-2} μm/√hour. For a 50,000hr exposure at 800^{o}C, this would also lead to a little more than an ~10μm effective scale thickness of Cr_2O_3. Thick scales are very likely to spall off, as the oxidation of the uncoated steel shows. An additional requirement for the coating and the scale that it forms on oxidation is that the area specific contact resistance (ASR), has to remain within acceptable limits.

3.4. Scale microstructures

Optical microscopy (KEYENCE VH-Z450 optical microscope) of the surfaces of the uncoated steel, Sample type A, after a 120hr cyclic oxidation at 850^{o}C clearly showed extensive spalling of the scale, Fig.4a; the apparently low oxidation rate of the unprotected steel (sample type A- Fig 2) is therefore the result of repeated spalling/reoxidation events, in which scale regrowth starts again after the scale is removed. Scale spalling was almost complete upon cooling sample type A once to room temperature after a 120hr isothermal oxidation at 850^{o}C, due to the formation of much thicker scale, Fig 4b. However, for oxidations at 800^{o}C up to 180 hrs, the scale was retained for sample type A (not coated), so that meaningful resistivity measurements could be made.

Cross sectional chemical analyses of the scale compositions were carried out in a ISI DI30C scanning electron microscope equipped with an EDX (energy dispersing X-ray) analytical system. To avoid electrical charging, all samples were coated with Au-Pd alloy in a Pelco Model 3 sputtering coater.

The results for a Type A sample (no coating) oxidized for 60 hrs at 800^{o}C + 120 hrs isothermally at 850^{o}C, and for a Type C sample (coated-compacted) after 60 hrs at 800^{o}C + a cumulative cyclic oxidation of 120hrs at 850^{o}C, are shown in Figs. 5a and b, respectively. The chemical analysis for Fig 5a was obtained from a fragment of the rough scale that still adhered. The oxide layer for sample Type A is about 5μm thick, and consists of a chromia sub-scale under an outer manganese-chromia spinel layer. The manganese in this case came from the 430 SS alloy itself, due to its high mobility and high oxidation potential. Formation of a $(Mn,Cr)_3O_4$ spinel in contact with a manganese-containing Cr_2O_3 scale is in agreement with the known phase relationships at this temperature, as determined by Speidel and Muan [22], where the Mn-Cr stability field extends to a ~40/60 Mn/Cr composition in air. The chromia subscale on the coated alloy (sample type C) oxidized at 850 ^{o}C, Fig. 6b is only of submicron thickness; the exact

thickness cannot be determined accurately form the EDX traces, due to the convolution of the compositional measurements resulting form the finite width of the electron beam probe (~ 1μm in diameter). The EDX line scans indicate that Cr has been incorporated to some extent into the coating, but at a concentration significantly lower than for Cr_2O_3. This suggests that Cr evaporation may be expected to be strongly reduced as well, but direct measurements of Cr loss remain to be made.

3.5. Areas Specific Resistances (ASRs)

The electrical resistances of sample type C (coated), after thermal cycling, and Sample A (uncoated 430SS) held isothermally at 800°C for 180 hours in air, were measured every 50°C from about 600°C to 800°C by the four-probe method. The results are shown in Fig. 6. Apparent activation energies for the ASRs, $E_{a,el}$ (eV), were obtained by fitting to an Arrhenius expression: $ASR(\Omega cm^2)=(B.T).exp\ (E_{a,el}/kT)$, where T is the temperature, k is the Boltzmann constant, and $B(\Omega cm^2K^{-1})$ is a constant. The ASRs decrease with increasing temperatures because the scales are n-type semiconductors. The temperature dependence of the ASR can be characterized by activation energies generally between 0.85 and about 1 eV. It is intriguing that the ASRs of the samples, with the exception of the uncoated steel oxidized for 180 hrs at 800°C , are clustered around the same values.

The ASRs of the uncoated 430SS fired at 800°C for 180 hours are about one order of magnitude higher than those of the coated samples, Fig.7. The ASR for the coated sample, initially oxidized for 60 hrs at 800°C, followed by an additional cyclic oxidation at 850°C for 120 hrs, is as low as $2.5x10^{-3}$ $ohmcm^2$. This is the lowest value obtained so far for a coated 430 SS at 850°C, particularly under similar thermal cycling conditions.

3.5 Mechanisms

The oxidation rate measurements and EDX data suggest plausible mechanisms for the oxidation of the coated and the uncoated samples. For the unprotected steel, during the initial oxidation Mn in the alloy is preferentially oxidized, leading to the formation a Mn-Cr spinel surface layer that is not protective, and continued oxidation forms a Mn-containing Cr_2O_3 scale that grows essentially unimpeded. For the coated steel, the dense Mn-Co-O layer has several beneficial effects: it eliminates the oxidation of Mn in the alloy, since the oxygen potential at the coating/alloy interface is effectively lowered; it significantly reduces the chromia subscale growth by blocking oxygen ingress; it improves the overall coating adherence, probably due to the formation of a thinner and more compact Cr_2O_3 scale; it introduces Co in the overall oxide layer on the alloy surface, which has the effect of significantly increasing its electronic conductivity, as well as lowering the thermal expansion to values more compatible with that of the steel.

3.6 ASR, contact geometry, and scale thickness

Simplified models can be used to estimate the effects of partial contact of the oxidized metal alloy with an SOFC electrode. In the strip-contact model, Fig. 7 a and b, part of the current during cell operation, I_a, is assumed to flow from the contact directly and uniformly into the alloy over a contact width a+δ, where δ is the scale thickness, while the second part of the overall current, I(x), is assumed to flow laterally through the scale to a distance x, where it enters the alloy over an area again of width δ, leading to a local current density, $i(x)= I(x)/(\delta\ell)$, where ℓ is the contact length. The total current for the contact of width a, length ℓ and a separation distance 2L between contacts, I_L, with

$$I_L = I_a + \int_{\delta}^{L} i(x)\,dx$$

may then be compared to that of a uniformly covering contact, $I_{uniform}$, so that

$I_L/I_{uniform}= Y(m,k)$, with $m=a/\delta$ and $k=L/\delta$.

It is then readily shown that

$Y(m,k)= (m+1)/(m+k) + (1/(m+k)).\ln k$,

a simple geometrical factor, independent of the scale's specific resistance, R_0.

While an exact calculation can be made using finite element analysis, the present simplified model is sufficient to estimate the effects of the general contact geometry that is shown in Fig 7b. It is clear that for $L/\delta > 10$ the averaged interface resistance would be significantly above that for uniform contact. The half-separation, L, between contacts could, for example be regarded as a channel width for air flow, or as the contact spacing of a porous electrode. For large values of L/δ the effective interface resistance would be increased by a factor of about 10 compared to uniform contact. As a further illustration, for $L/\delta > 30$, and $m=a/\delta < 1$, Y(m,k) is not very sensitive to L/δ, which leads to the conclusion that for an increasing δ at constant L, the total ASR is approximately inversely proportional to $\sim [Y(m,k)^{-1}] x \delta x R_0$, or $10 x \delta x R_0$. This will require the oxidation scale to have a very low specific resistance if the average ASR is to remain below some acceptable level, such as 0.1 Ωcm^2 after 50,000hrs of operation.

A similarly simplified model may be used to evaluate the case of disk-shaped contacts of radius a, with edge to edge spacing L. Such a model leads to the approximate expression

$$Y(m,k) = (1/k)^2 (m+1)^2 + (1/k).ln(k/(m+1)).$$

Fig. 8 compares the approximate values for $m<1$, indicating that disk-type contacts lead to more significant increases in contact resistance compared to strip contacts, as may be intuitively expected. The significance of geometrical effects on contact resistance have been considered by numerous authors, [23-27] to varying degrees of approximations. The results are generally similar.

The dependence of the ASR on temperature and time may be expressed empirically as

$$ASR(t,T,Y) = [Y(m,k)]^{-1} R_o k_{p\ eff} \sqrt{t}$$

For the coatings developed here, an oxidation of 60hrs at 800^{o}C+120 hrs at 850^{o}C led to an ASR of $2.3 x 10^{-3}$ Ωcm^2. With $[Y(m,k)]^{-1}=10$ this would predict an ASR after 50,000 hrs at 850^{0}C of approximately $0.5 \Omega cm^2$.

The following strategies for reaching tolerable contact resistances can be considered:

- Introduce various doping elements to reduce R_o further
- Changing the contact geometry to increase Y(m,k)
- Changing the temperature of operation
- Using alloys such as Plansee or ODS alloys, with materials and processing cost penalty

As discussed by Huang *et al.*, [14] the benefit of reducing the temperature of operation of the fuel cell will depend on the effective activation energies of $k_{p\,eff}$ and R_o, $E_{a,ox}$ and $E_{a,el}$, with $E_{a,ox} \propto ½\, ln\, k_g$. Obviously, benefit at lower temperatures only results if $E_{a,ox} > E_{a,el}$. Activation energies for oxidation of various Fe-Cr -containing alloys have been determined by several authors. While these do not necessarily apply to the steel protected by a complex scale, it is reasonable to assume that they will generally be of comparable magnitude in the present case. Brylewski *et al*. [23] cite activation energies of about 200 kJ/mole, *i.e*. about 2eV. Under these conditions, with $E_{a,ox}$ about 1eV, a lowering of the temperature of operation to 700^{o}C would bring the ASR down to below 0.1Ωcm^2 even if Y(m,k)~0.1.While further measurements, particularly for extended times at lower temperatures remain to be made, the analysis provides a plausible argument for reducing the operating temperatures of SOFCs that use protected coating on ferritic stainless steels, such as the 430SS used here, to 700^{0}C or below.

4. Conclusions

1. An effective, dense and well adherent coating was produced on 430SS that has the result of significantly reducing the oxidation rate of the alloy. The coating is essentially a Mn-Co-O spinel, applied in powder form, and compacted to improve its green density.

2. A simplified model has been presented that allows an assessment of the effects of the contact and scale geometries.

3. For 850^{o}C, an ASR can be predicted of approximately 0.5Ωcm^2, after 50,000hrs in air, taking into account a factor of 10 penalty for unfavorable contact geometries.

4. The effect of the densified Mn-Co spinel coating is to reduce significantly Cr_2O_3 sub-scale formation, lower the thermal expansion mismatch, and increase the electronic conductivity of the scale.

5. The findings point to several potential remedies for achieving coatings on commercial stainless steel alloys that allow for metal interconnects with a service life of 50,000hrs or more. Considering contact geometries, such service life is unlikely to be possible above operating temperatures of about 700^{o}C, unless highly specialized alloys are used, with potential processing and cost penalties.

5. Acknowledgements

This work was supported by the U.S. Department of Energy, National Energy Technology Laboratory. Additional support was provided by the U.S. Department of Energy under Contract No. DE-AC03-76SF0098.

6. References

1. S. de Souza, S. J. Visco and L. C. De Jonghe, *Solid State Ionics*, 98, 571 (1997).

2. S. de Souza, S. J.Visco and L.C.De Jonghe, *Journal of Electrochem. Soc.* 144, L35 (1997).

3. J-W Kim, A. V. Virkar, K-Z Fung, K. Mehta, and S. C. Singhal, *J. Electrochem. Soc.*, **146**, 69 (1999).

4. H. Ishihara, H. Matsuda and Y. Takita, *J. Am. Chem. Soc*., **116**, 3801 (1994).

5. M. Feng and J. B. Goodenough, Eru. *J. Solid State Inorg. Chem.*, **T31**, 663 (1994)

6. K. Q. Hung, R. Tichy and J. B. Goudenough, *J. Am. Ceram. Soc*., **81**, 2565 (1998)

7. W. J. Quadakkers, H. Greiner and W. Kock, in *Proc.1st European SOFC Forum*, U. Bossel, Ed., p. 525, Lucerne, Switzerland (1994).

8. W. J. Quadakkers, H. Greiner, M. Hansel, A. Pattanaik, A.S. Khanna, W. Mallener, *Solid State Ionics*, **91**. 55 (1996).

9. S. Linderoth, P.V. Hendriksen and M. Mogensen, *J. Mat. Sci.*, **31**, 5077 (1996).

10. N. Q. Minh, T. Takahashi, Science and Technology of Ceramic Fuel Cells, Elsevier, Amsterdam, 1995.

11. H. Asteman, J.-E. Svensson, L.-G. Johansson, M. Norell, *Oxid. Met.* **52,** 95(1999).

12. S.P. Jiang, J.P. Zhang, X.G. Zheng, *J. Eur. Ceram. Soc*., **22,** 361(2002).

13. P.Y. Hou, K. Huang and W. Bakker. *Proc. 6th International Symposium on Solid Oxide Fuel Cells*, Honolulu, Havaii, Oct. 17-22, 1999.

14. K. Huang, P. Hou, J. B. Goodenough, *Solid State Ionics*, **129,** 237(2000).

15. D. G. Wickham, W. J. Croft, *J. Phys. Chem.Solids* **7,** 351(1958).

16. S. Naka, M. Inagaki, T. Tanaka, *J. Mater. Sci*. **7,** 441(1972) .

17. Y. Larring and T. Norby, *J. Electrochem. Soc*, **147**(9) 3251-3256 (2000).

18. S. Badwal, K. Foger, X. G. Zheng, and D. Jaffrey, US patent 5,942,349, August 24, 1999

19. L.A. Chick, L.R. Pederson, G.D. Maupin, J.L. Bates, L.E. Thomas, G.J. Exarhos, *Mater. Lett.* **10**, 6 (1990).

20. H. Nagai, T. Fujikawa, K. Shoji, *Trans. Japan Inst. Met*. **24,** 581(1983).

21. J.H.Zhu, Y. Zhang, A.Basu, Z.G.Lu, M. Paranthaman, D.F. Lee, and E.A. Payzant, *Surface and Coatings Technology*, **177-178**, 65(2004).

22. D.H. Speidel and A. Muan, *J. Amer Ceram. Soc.*, **46**, 578(1963).

23. R. Holm, Electric Contacts, Chap. 1, Springer-Verlag, NY, 1967.

23. E. Gorin and H.L. Recht, in *" Fuel Cells"*, pp 193-252, 1963. W. Mitchell, Ed., Academic Press, NY 1963.

24. J. Fleig and J. Maier, *Electrochim. Acta* **41**(7/8), 1003-1009 (1996).

25. J. Fleig and J. Maier, *Solid State Ionics*, **85**, 17(1996).

26. J. Fleig and J. Maier, *Solid State Ionics*, **86-88**, 1351 (1996).

27. E. Wanzenberg, F. Tietza, D. Kek, P. Panjan, D. Stöver, *Solid State Ionics*, **164,** 121(2003).

28. T. Brylewski, M. Nanko, T. Maruyama, K. Przybylski, *Solid State Ionics*, **143,**131**(**2001).

TABLES

Table 1.

Stainless steel composition in Weight%

Element	Cr	C	Ni	Mn	Si	Fe
wt%	16.3	0.04	0.2	0.45	0.40	balance

Table 2.

material	ΔCTE x10^6
LSM (CTE:12x$10^{-6}K^{-1}$)	0
$MnCo_2O_4$	-0.3
$MnCoCrO_4$	-3.1
$MnCr_2O_4$;$Mn_{1.5}Cr_{1.5}O_4$	-6.7
Cr_2O_3	-6.5
430 SS	-0.6

Table 3.

	Oxidation Temp. (^oC)	k_g ($g^2cm^{-4}s^{-1}$)	k_p ($\mu m/\sqrt{hr}$)
Sample A	850	1.28x10^{-12}	5.0x10^{-1}
Sample C	850	1.48x10^{-14}	4.4x10^{-2}

FIGURE CAPTIONS:

Fig.1 Conductivities of oxides as a function of temperature, with corresponding activation energies in eV. The Cr_2O_3 value is from Ref. 20.

Fig.2. Cross-sectional SEM images, comparing the structure of as deposited and compacted coatings after an initial heat treatment in air at 800^{o}C for 60 hrs. The compacted coating has formed a dense layer, while the uncompacted one has not.

Fig.3. Weight gain of uncoated and coated samples, Type A and C respectively, during isothermal heating or cyclic oxidation at 850^{o}C, following an initial oxidation at 800^{o}C for 60hrs. Weight gains during the heating and cooling periods are not taken into account. The coated samples have a dramatically reduced rate of weight gain. *(or delete the last two sentences).*

Fig. 4 Surface, (a) Optical and (b) SEM, images of 430 SS heated at 800^{o}C/60hr +120hrs isothermally at 850^{o}C, after cooling to room temperature. Spalling is extensive.

Fig. 5 EDX traces (dotted lines) of scales on samples oxidized at 800^{o}C/60hr +120hrs isothermally at 850^{o}C;
a: oxidized uncoated steel; note the Mn/Cr oxide scale over the chromia subscale.
b: oxidized coated steel, Type C; the Chromia sub-scale is still sub-micron. Note also the low Cr content of the outer scale.

Fig. 6. Electrical resistivities as a function of temperature for the various samples, with corresponding effective activation energies. The activation energies are generally less than 1 eV.

Fig 7. Simplified model geometry for assessing the effects of contact geometry on the average contact resistance. When the contact spacing get large compared to the scale thickness, the geometric penalty, proportional toY^{-1}, becomes rapidly large.

Fig. 8. Simplified model geometry for assessing the effects of disk contact geometry on the average contact resistance. The effects are significantly more pronounced than for strip contacts.

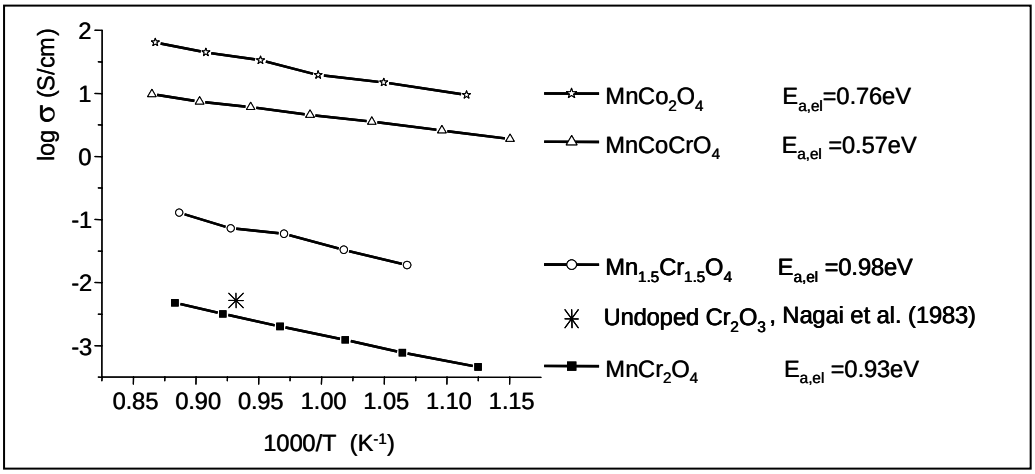
log σ (S/cm)
2
1
0
-1
-2
-3
0.85
0.90
0.95
1.00
1.05
1.10
1.15
1000/T (K-1)
MnCo2O4 Ea,el=0.76eV
MnCoCrO4 Ea,el =0.57eV
Mn1.5Cr1.5O4 Ea,el =0.98eV
Undoped Cr2O3 , Nagai et al. (1983)
MnCr2O4 Ea,el =0.93eV

fig 1

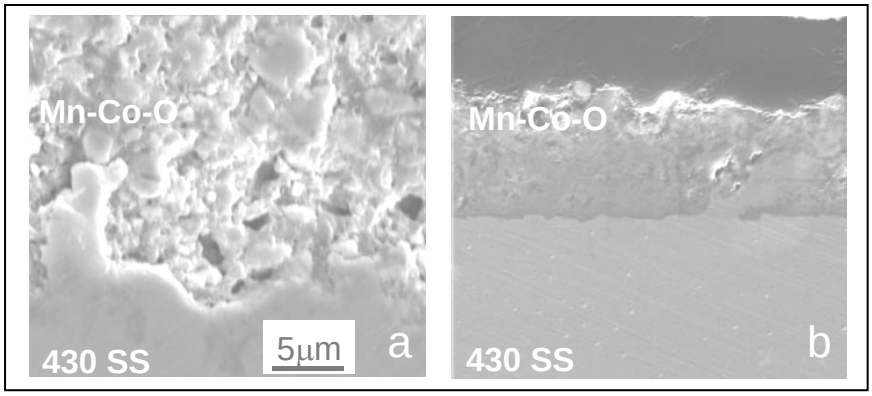

Fig 2

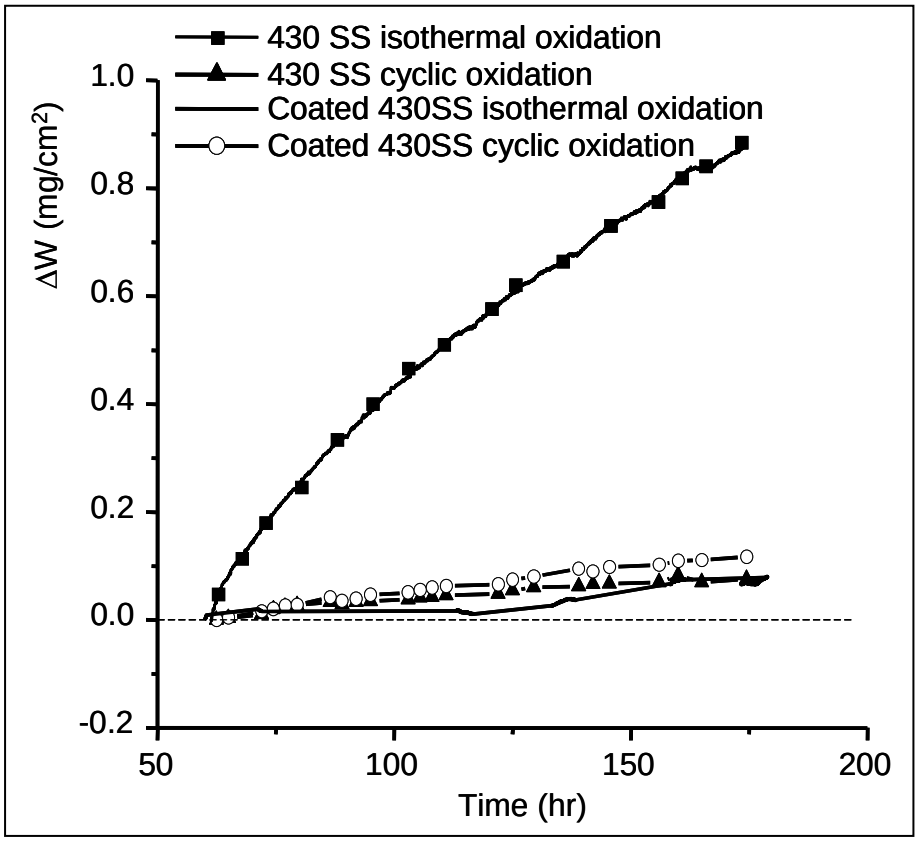
430 SS isothermal oxidation
430 SS cyclic oxidation
Coated 430SS isothermal oxidation
Coated 430SS cyclic oxidation
ΔW (mg/cm²)
1.0
0.8
0.6
0.4
0.2
0.0
-0.2
50
100
150
200
Time (hr)

fig 3

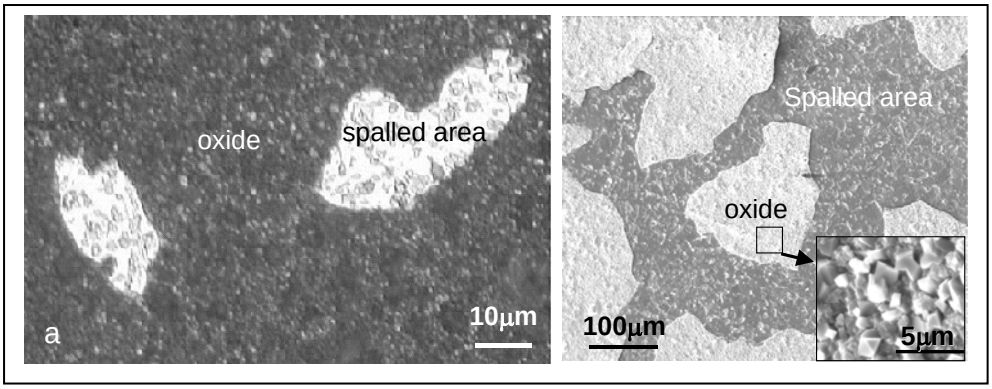

fig 4 a and b

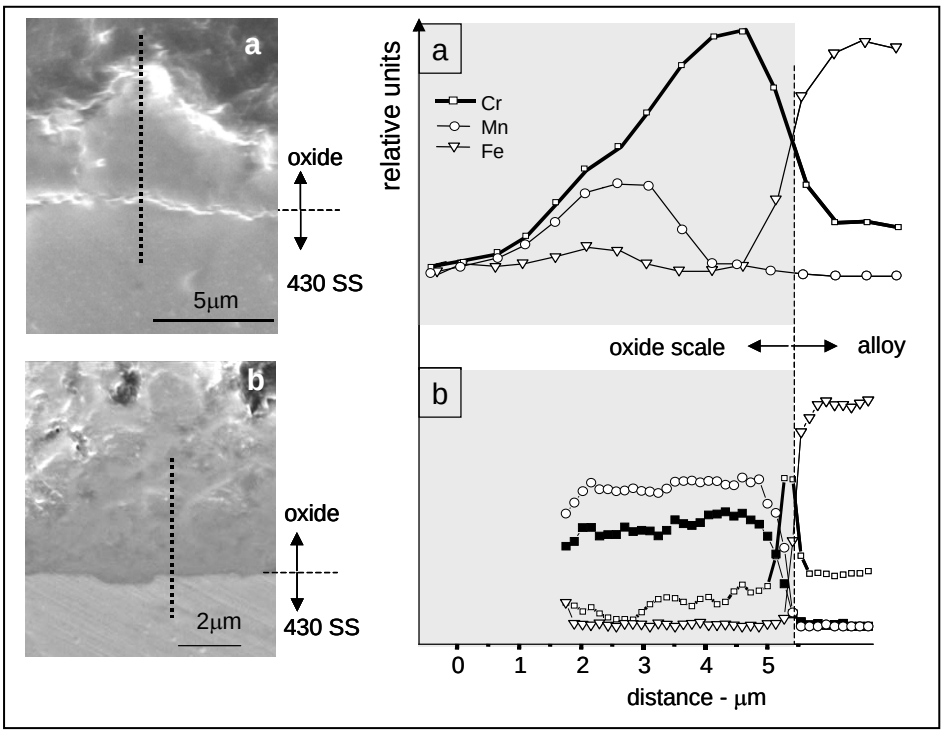
a
oxide
430 SS
5μm
b
oxide
430 SS
2μm
relative units
a
Cr
Mn
Fe
oxide scale
alloy
b
0
1
2
3
4
5
distance - μm

fig 5, a,b

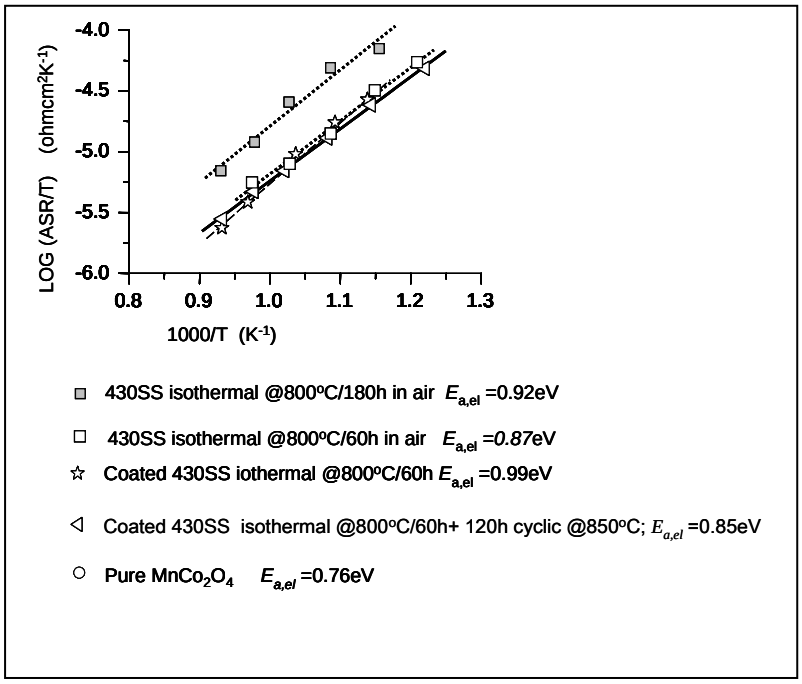
-4.0
-4.5
-5.0
-5.5
-6.0
LOG (ASR/T) (ohmcm²K⁻¹)
0.8
0.9
1.0
1.1
1.2
1.3
1000/T (K⁻¹)
430SS isothermal @800ºC/180h in air Ea,el =0.92eV
430SS isothermal @800ºC/60h in air Ea,el =0.87eV
Coated 430SS iothermal @800ºC/60h Ea,el =0.99eV
Coated 430SS isothermal @800ºC/60h+ 120h cyclic @850ºC; Ea,el =0.85eV
Pure MnCo2O4 Ea,el =0.76eV

fig6

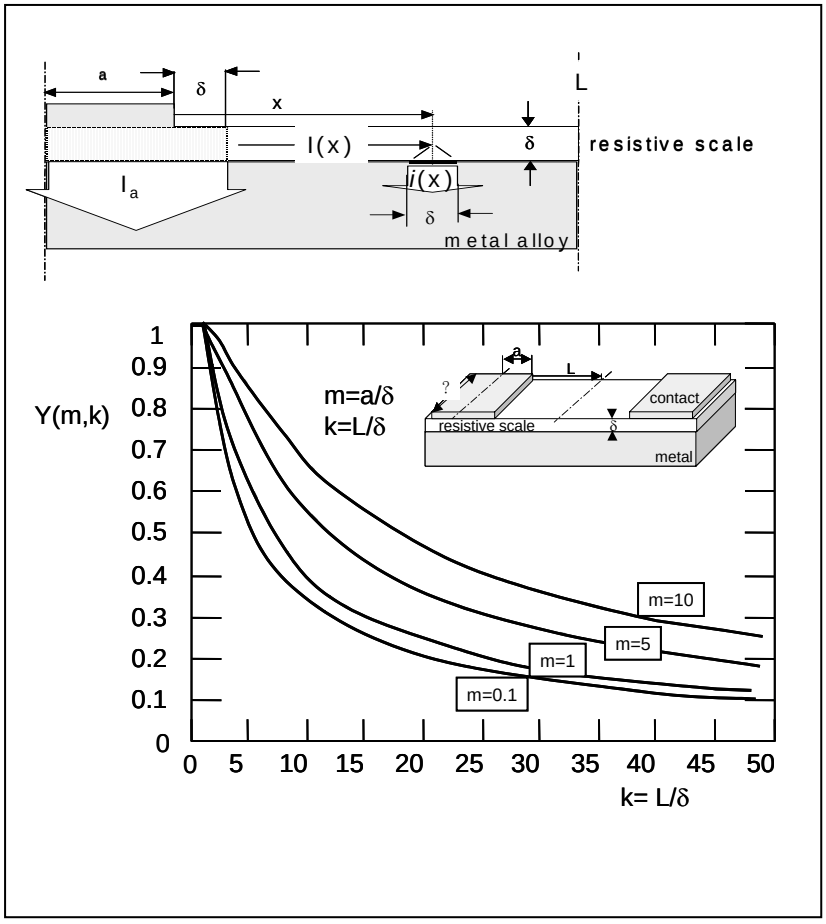

fig 7a (top),b(bottom)

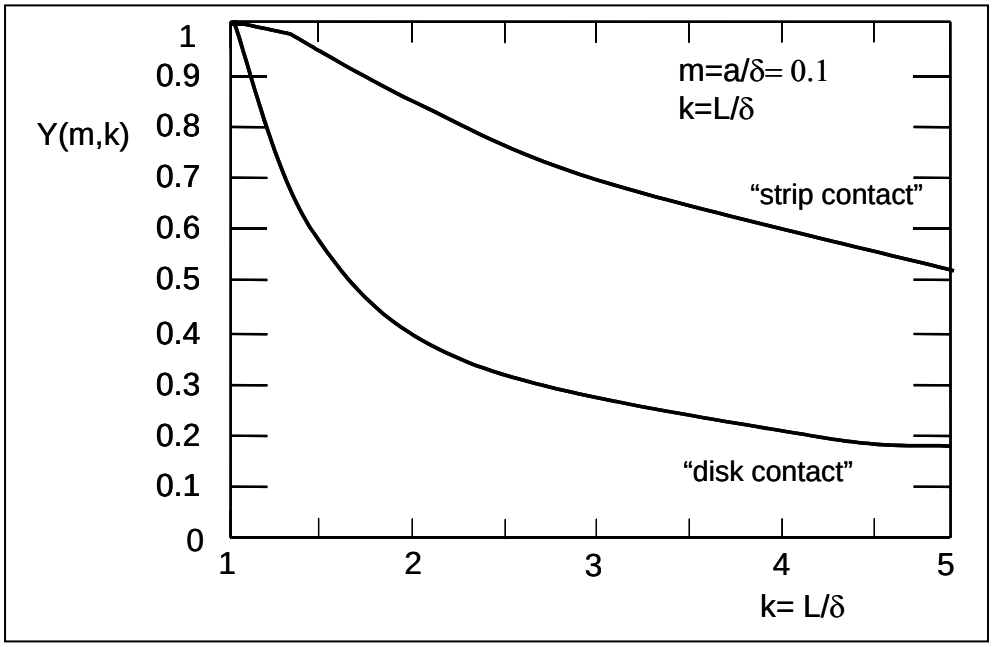
Y(m,k)
1
0.9
0.8
0.7
0.6
0.5
0.4
0.3
0.2
0.1
0
1
2
3
4
5
m=a/δ= 0.1
k=L/δ
“strip contact”
“disk contact”
k= L/δ

Fig 8.